# Remotely sensing phytoplankton size structure in the Red Sea

John A. Gittings[a*], Robert J. W. Brewin [b,c], Dionysios. E. Raitsos [c,d], Malika Kheireddine [e], Mustapha Ouhssain[e], Burton H. Jones[e], Ibrahim Hoteit[a*]

[a] King Abdullah University of Science and Technology (KAUST), Department of Earth Science and Engineering, Thuwal, 23955-6900, Kingdom of Saudi Arabia

[b] College of Life and Environmental Sciences, University of Exeter, Penryn Campus, Penryn, TR10 9FE, United Kingdom

[c] Plymouth Marine Laboratory (PML), The Hoe, Plymouth, PL1 3DH, United Kingdom

[d] Department of Biology, National and Kapodistrian University of Athens, Athens, Greece

[e] King Abdullah University of Science and Technology (KAUST), Red Sea Research Center, Biological and Environmental Science and Engineering Division, Thuwal, 23955-6900, Kingdom of Saudi Arabia

## ABSTRACT

Phytoplankton size structure impacts ocean food-web dynamics and biogeochemical cycling, and is thus an important ecological indicator that can be utilised to quantitatively evaluate the state of marine ecosystems. Potential alterations to size structure are predicted to occur in tropical regions under future scenarios of climate change. Therefore, there is an increasing requirement for the synoptic monitoring of phytoplankton size structure in marine systems. The Red Sea remains a comparatively unexplored tropical marine ecosystem, particularly with regards to its large-scale biological dynamics. Using an *in situ* pigment dataset acquired in the Red Sea, we parameterise a two-component,

abundance-based phytoplankton size model and apply it to remotely-sensed observations of chlorophyll-a (Chl-a) concentration, to infer Chl-a in two size classes of phytoplankton, small cells < 2μm in size (picophytoplankton) and large cells > 2μm in size. Satellite-derived estimates of phytoplankton size structure are in good agreement with corresponding *in situ* measurements and also capture the spatial variability related to regional mesoscale dynamics. Our analysis reveals that, for the estimation of Chl-a in the two size classes, the model performs comparably or in some cases better, to validations in other oceanic regions. Our model parameterisation will be useful for future studies on the seasonal and interannual variability of phytoplankton size classes in the Red Sea, which may ultimately be relevant for understanding trophic linkages between phytoplankton size structure and fisheries, and the development of marine management strategies.

Keywords: ocean colour, remote sensing, phytoplankton, size structure, chlorophyll, Red Sea

## 1. INTRODUCTION

Ecological indicators, which may be defined as quantifiable metrics that characterise ecosystem structure, composition or function, can be used to monitor the state of marine ecosystems and their response to environmental perturbations (*Niemi and Mcdonald*, 2004; *Platt and Sathyendranath, 2008; Racault et al*. 2014). In the global oceans, commonly used indicators are typically based on the presence and distribution of phytoplankton (as indexed by the concentration of chlorophyll-a [Chl-a]), which form the

53 base of oceanic food webs. Among the ecological indicators that can be derived from
54 observations of ocean colour (e.g. primary production and phytoplankton phenology), the
55 size structure of phytoplankton communities is particularly important as it can influence
56 marine food web structure (*Legendre and Le Fèvre, 1991*; *Maloney and Field, 1991*;
57 *Parsons and Lalli, 2002*), biogeochemical cycling (*Chisholm, 1992*), carbon export (*Boyd*
58 *and Newton, 1999; Briggs et al. 2011*; *Eppley and Peterson, 1979; Guidi et al. 2009;*
59 *Laws et al. 2000; McCave, 1975*) and the thermal structure of the upper-oceanic layer
60 (*Sathyendranath and Platt, 2007*).

61 The Red Sea, situated between the African continent and Arabian Peninsula, is the
62 world's northernmost tropical sea. It hosts coral reef ecosystems, contains high levels of
63 marine biodiversity, and supports shipping, fisheries and tourism, making it a vital
64 economic asset to the region (*Berumen et al. 2013*; *Carvalho et al. 2019; Gladstone et al.*
65 *2013*). Over the last decade, the Red Sea has been subject to regional warming (*Chaidez*
66 *et al. 2017; Krokos et al. 2019; Raitsos et al. 2011*), linked with coral reef bleaching
67 events (*Cantin et al. 2010*; *Monroe et al. 2018; Osman et al. 2018*), and alterations in
68 phytoplankton abundance and phenology (*Gittings et al. 2018; Raitsos et al. 2015*).
69 Consequently, there is a need to monitor the response of the Red Sea ecosystem to future
70 climate variability.

71 Due to limited *in situ* sampling, knowledge on the spatiotemporal distribution of
72 phytoplankton size structure in the Red Sea is relatively sparse. Nevertheless, increased
73 *in situ* sampling efforts over the last two decades have enabled researchers to gain insight
74 in localised regions of the Red Sea, including the Gulf of Aqaba (*Shaikh et al 1986;*
75 *Sommer et al. 2002*), the central east coast (*Al-Najjar et al. 2007; Touliabah et al. 2010*)

and the north-western Red Sea (*Nassar et al.* 2014). More recently, *Pearman et al*. (2016) used a molecular approach to assess phytoplankton community structure in the northern and southern ends of the Red Sea, and *Kheireddine et al.* (*2017*) used a taxonomic, pigment-based approach to investigate community structure along the central axis of the basin. Both studies revealed that pico-phytoplankton were the main contributor to the total phytoplankton biomass, although the relative contributions of pico-, nano- and micro-phytoplankton varied with environmental conditions and mesoscale features. For extensive reviews on phytoplankton species composition in the Red Sea, the reader is referred to the works of *Ismael* (2015) and *Qurban et al*. (2019).

A key method used to observe ecological indicators synoptically and frequently is ocean-colour remote sensing (*Platt 2008, Platt et al. 2009*), and several studies have demonstrated the applicability of satellite remote sensing for investigating the spatiotemporal distribution of phytoplankton abundance in the Red Sea (*Acker et al. 2008; Brewin et al. 2013, 2015a; Dreano et al. 2016; Gittings et al. 2018, 2019; Papadopoulos et al. 2015; Racault et al. 2015; Raitsos et al. 2013, 2015, 2017*; *Triantafyllou et al. 2014*). Existing remote-sensing methodologies for deriving phytoplankton size classes (PSCs) can be broadly categorised into abundance-based (*Brewin et al.* 2010, 2011; *Hirata et al*. 2011; *Uitz et al*. 2006) and spectral-based (*Devred et al.* 2011; *Kostadinov et al*. 2009) approaches. A detailed review of these different methods can be found in *IOCCG* (2014), *Bracher et al*. (2017) and *Mouw et al*. (2017). Recent inter-comparisons have revealed that abundance-based approaches, which exploit the ubiquitous relationship between phytoplankton biomass and cell size (lower biomass equates to smaller cell size and vice versa, (*Chisholm, 1992*)), performs well at

retrieving PSCs (*Hu et al. 2018; Liu et al. 2018*). Specifically, the three-component PSC model of *Brewin et al.* (2010), which builds upon the work of *Sathyendranath et al.* (2001) and *Devred et al.* (2006), was shown to perform well in these inter-comparisons, and has been successfully re-parameterised and validated in many other oceanic regions, including: the Atlantic Ocean (*Brewin et al. 2010*; *Brotas et al., 2013*), the Indian Ocean (*Brewin et al. 2012a*), the South China Sea (*Lin et al. 2014*), the continental shelf seas of China (*Sun et al. 2018*), the Western Iberian coastline (*Brito et al. 2015*), the Mediterranean Sea (*Sammartino et al. 2015*), Southern Africa (*Lamont et al. 2008*), Chile (*Corredor-Acosta et al. 2018*) and the global ocean (*Brewin et al. 2015b*; *Ward, 2015*).

Recently, *Brewin et al.* (2015a) applied this model to derive pico- (< 2 μm) and combined nano/micro- (> 2 μm) phytoplankton size classes in the Red Sea. However, due to the paucity of *in situ* data on these two size classes within the region, at the time, their study utilised model parameters obtained from other oceanic regions (see *Brotas et al. 2013*), justified through analysis of particulate absorption data collected in the Red Sea. Since then, *in situ* datasets have become available, enabling the characterisation of phytoplankton size structure in the Red Sea over large spatial scales (*Kheireddine et al. 2017, 2018a*). In this study, we utilise these newly available datasets to test and subsequently re-parameterise the PSC model of *Brewin et al.* (2015a) for the first time in the Red Sea. We then apply this model to ocean-colour observations and provide a series of examples demonstrating the improved performance of the updated approach.

## 2. DATA AND METHODOLOGY

### *2.1 Oceanographic cruises and sampling*

Seawater samples were acquired during five research cruises conducted across the Red Sea between October 2014 and January 2016 aboard the *R/V Thuwal* (*Kheireddine et al. 2017, 2018a*) (Fig. 1, Table 1). Collectively, these cruises spanned the majority of the Red Sea (latitudinal range of ~ 15°N – 27°N) and, for convenience, can be separated into the following biogeographical regions: the Northern Red Sea (NRS), Central Red Sea (CRS) and Southern Red Sea (SRS).

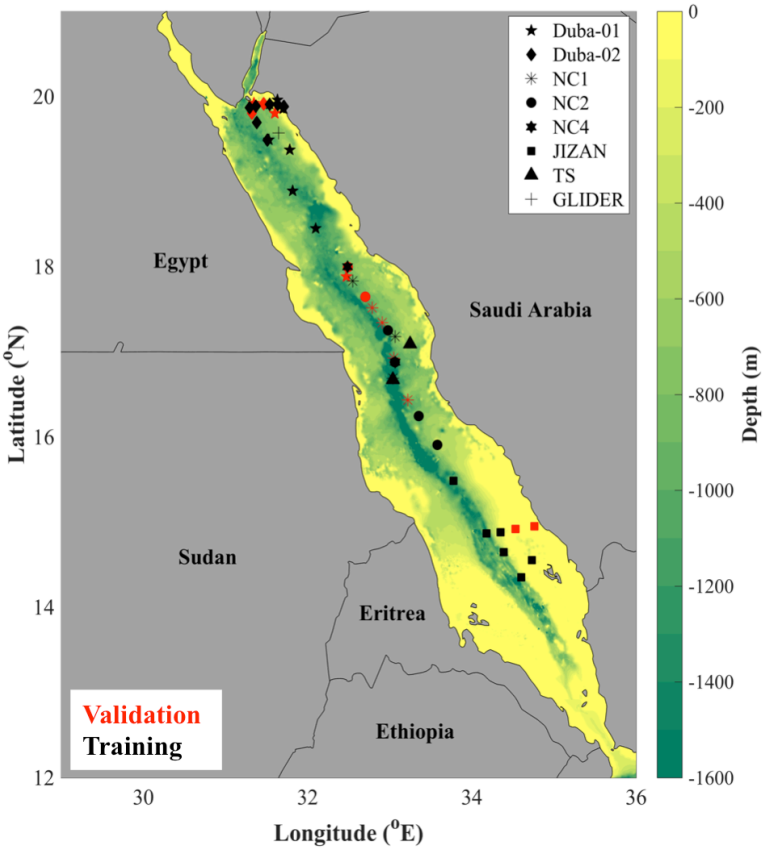

**Figure 1.** Map displaying the bathymetry of the Red Sea and the locations of the cruise sampling stations. Markers in red and black represent the data used for the validation and training of the phytoplankton size class model respectively.

A total of 49 stations were sampled over the Red Sea, although we note that two of these stations were repeated locations sampled on different days. The biogeographic region and temporal period associated with each of the cruises is presented in Table 1 and described in further detail by *Kheireddine et al.* (2018a).

**Table 1.** Summary of the Red Sea cruises and *in situ* datasets

| Cruise Campaign | Vessel | Location | Abbreviation | Time Period | Number of stations | Number of samples | Number of satellite match-ups |
|---|---|---|---|---|---|---|---|
| Duba Cruise 1 | *RV Thuwal* | Northern Red Sea | Duba-01 | 17 - 28 Apr 2015 | 10 | 24 | 3 |
| Duba Cruise 2 | *RV Thuwal* | Northern Red Sea | Duba-02 | 21 Mar - 2 Apr 2016 | 10 | 28 | 2 |
| Nutrient Cycle Cruise 1 | *RV Thuwal* | Central Red Sea | NC1 | 16 - 28 Oct 2014 | 7 | 16 | 4 |
| Nutrient Cycle Cruise 2 | *RV Thuwal* | Central Red Sea | NC2 | 3 - 9 Apr 2015 | 6 | 18 | 2 |
| Nutrient Cycle Cruise 4 | *RV Thuwal* | Central Red Sea | NC4 | 17 - 28 Jan 2016 | 2 | 6 | - |
| Jizan | *RV Thuwal* | Southern Red Sea | JIZAN | 8 - 21 Feb 2015 | 8 | 27 | 2 |
| Time Series | *RV Thuwal* | Central Red Sea | TS | Ongoing from 3 Dec 2014 - 12 Sept 2015 | 5 | 11 | 1 |
| Seaglider AUV | *Autonomous Glider* | Northern Red Sea | GLIDER | 25 Mar 2015 | 1 | 3 | - |
| **Total** | | | | | **49** | **133** | **14** |

*2.2 Phytoplankton pigment database*

Briefly, at each sampling station, seawater samples (volume ranging from 2.4 – 2.8 L) were collected within the upper 200 metres of the water column and filtered through 25 mm diameter Whatman GF/F filters (porosity of 0.7 μm). The filters were flash frozen and stored in liquid nitrogen throughout the cruise, then transferred to an -80°C freezer in the laboratory prior to analysis. Samples were extracted in 3 mL of 100% methanol,

disturbed with glass pearls on a cooled vibratory homogenizer, centrifuged, and filtered 2 h later using a Teflon syringe filter (0.2 μm). Within 24 hours, the sample extracts were analysed by High Performance Liquid Chromatography (HPLC) using a complete 1,260 Agilent Technologies system. Measurements of photosynthetic phytoplankton pigments were acquired in accordance with the HPLC analytical procedure followed by *Ras et al.* (2008) and as described by *Kheireddine et al.* (2017, 2018a). Only samples within the upper 20 metres of the water column for each station were selected for the analysis, as satellite sensors acquire measurements approximately within the first optical depth (typically around 20 meters in the Red Sea (*Raitsos et al.* 2013)). Uncertainties associated with the determination of pigment concentrations were calculated using the principles of uncertainty propagation and are provided in *Kheireddine et al*. (2017).

*2.3 Estimation of phytoplankton size structure from HPLC data*

For estimating phytoplankton size fractions from HPLC data, we used the method of *Brewin et al*. (2015b), adapted from *Claustre* (1994), *Vidussi et al*. (2001), *Uitz et al*. (2006), *Brewin et al*. (2010) and *Devred et al.* (2011). First, the total Chl-a concentration ($C$) was computed from the weighted sum of seven diagnostic phytoplankton pigments (henceforth referred to as $C_w$), according to

$$C_w = \sum_{i=1}^{7} W_i \, P_i \quad (1),$$

where **W** represents the weights and **P** corresponds to the following seven diagnostic pigments: fucoxanthin, peridinin, 19′-hexanoyloxyfucoxanthin, 19′-butanoyloxyfucoxanthin, alloxanthin, total chlorophyll-b and zeaxanthin. We estimated **W** by applying a multi-linear regression on the 133 samples collected during the five cruises. We then compared our weights with previous studies conducted in other regions of the global oceans (Table 2). The computed weights are in reasonable agreement with other datasets, with the exception of notable differences observed for the weights attributed to peridinin and alloxanthin. We speculate that the differences in these particular pigments were related to their very low concentrations during sampling. As only a small number of samples (133) were used to compute the weights, when compared with other published studies (e.g. *Uitz et al.* 2006; *Brewin et al.* 2015b), and considering the potentially erroneous values obtained with the re-parameterisation, we also tested weights derived from multiple studies across different regions (Table 2). Excluding our own re-parameterised weights, the weights computed by *Brewin et al.* (2014a) gave the overall best statistical performance with regards to the relationship between $C_w$ and total Chl-a ($C$) (Supplementary Fig. 1). Accordingly, we used these weights in our analysis.

**Table 2.** Phytoplankton pigments and a comparison of the weights (**W**), computed for Equation 1 using the 133 HPLC data samples collected in this study, with weights derived from other studies.

| Pigment | This study | Brewin et al. (2014a) | Brewin et al. (2015b) | Brewin et al. (2017a) | Uitz et al. (2006) | Uitz et al. (2008) | Soppa et al. (2014) |
|---|---|---|---|---|---|---|---|
| Fucoxanthin | 1.18 (± 0.51) | 1.72 | 1.51 | 1.65 | 1.41 | 1.65 | 1.55 |
| Peridinin | 6.45 (± 2.60) | 1.27 | 1.35 | 1.04 | 1.41 | 1.3 | 0.41 |
| 19' - Hexanoyloxyfucoxanthin | 0.57 (± 0.61) | 0.68 | 0.95 | 0.78 | 1.27 | 0.83 | 0.86 |
| 19' - Butanoyloxyfucoxanthin | 3.15 (± 1.51) | 1.42 | 0.85 | 1.19 | 0.35 | 0.78 | 1.17 |
| Alloxanthin | 7.70 (± 3.37) | 4.96 | 2.71 | 3.14 | 0.6 | 0.73 | 2.39 |
| Total chlorophyll-b | 1.66 (± 0.57) | 0.81 | 1.27 | 1.38 | 1.01 | 0.77 | 1.06 |
| Zeaxanthin | 0.72 (± 0.13) | 1.28 | 0.93 | 1.02 | 0.86 | 1.29 | 2.04 |

Next, based on the previously reported finding that two optically-distinct assemblages of particles dominate the Red Sea, and that Chl-a in the Red Sea is generally lower than 1 mg $m^{-3}$ (*Brewin et al. 2015a*), we computed fractions of the total Chl-a concentration for two size classes: pico-phytoplankton (cell size < 2 μm) and combined nano/micro-phytoplankton (cell size > 2 μm). Due to a low contribution of micro-phytoplankton to total Chl-a in our dataset (figure not shown), a two-component model was selected for our study as a more parsimonious solution to the original three-component model put forth by *Brewin et al*. (2010). However, we do not rule out the future use of a three-component model in the region, should datasets become available that span a higher range of chlorophyll (e.g. in coastal waters). Following Eq. 2, the fraction of pico-phytoplankton ($F_p$) was computed using zeaxanthin, total chlorophyll-b and by apportioning some of 19-hexanoyloxyfucoxanthin to the pico-phytoplankton pool at total Chl-a concentrations less than 0.08 mg $m^{-3}$ (*Brewin et al*. 2010, 2015b)

$$F_p = \begin{cases} \frac{(-12.5C+1)W_3P_3}{C_w} + \frac{\sum_{i=6}^{7} W_iP_i}{C_w} & \text{if C } \leq \text{ 0.08 mg } m^{-3} \\ \frac{\sum_{i=6}^{7} W_iP_i}{C_w} & \text{if C } \geq \text{ 0.08 mg } m^{-3} \end{cases} \quad (2).$$

The fraction of Chl-a attributed to the combined nano/micro phytoplankton assemblage ($F_{n,m}$) was then computed as

$$F_{n,m} = 1 - F_p \quad (3).$$

After deriving the fractions of the picophytoplankton ($F_p$) and combined nano/micro ($F_{n,m}$) phytoplankton populations relative to total Chl-a, the Chl-a concentration attributed to the two size classes was calculated as

$$C_p = F_p C \quad (4)$$

and

$$C_{n,m} = F_{n,m} C \quad (5),$$

where $C_p$ and $C_{n,m}$ correspond to the size-specific Chl-a concentration of pico-phytoplankton and the combined nano/micro-phytoplankton respectively, and $C$ refers to the total Chl-a concentration.

*2.4 Datasets and data partitioning for training, satellite validation and visualisation*

The *in situ* samples were matched with estimates of satellite-derived remote sensing reflectance ($R_{rs}$) from version 3.1 of the European Space Agency's Ocean Colour Climate Change Initiative product (OC-CCI). For the period spanning 2015 - 2017, the OC-CCI product consists of merged and bias-corrected data from the Moderate Resolution Imaging Spectroradiometer (MODIS) and Visible Infrared Imaging Radiometer Suite (VIIRS) satellite sensors. Level 3, daily, mapped data were acquired at a spatial resolution of 4 km from http://www.esa-oceancolour-cci.org for the time periods

corresponding to each of the cruises (Table 1). For further information, the reader is referred to previous literature regarding the OC-CCI product (*Sathyendranath et al. 2012*, *2016*) and its previous applications in the Red Sea and adjacent Arabian Sea (*Racault et al. 2015*; *Brewin et al. 2015a*; *Dreano et al. 2016*; *Gittings et al. 2017*). In addition, we refer the reader to the OC-CCI Product User Guide at http://www.esa-oceancolour-cci.org/?q=webfm_send/318 for a more extensive overview of processing, sensor merging and uncertainty quantification. Each sample was matched to an individual satellite pixel temporally (same day) and spatially (nearest pixel based on longitude and latitude). Of the total 49 stations, we retrieved 14 satellite matchups. The corresponding sample stations for the matchups were set aside for the independent validation of satellite-derived total Chl-a, size fractions and size-specific Chl-a (Fig. 1). The *in situ* samples at each of the matchup stations were averaged within the top 20 metres (approximately the first optical depth). The remaining 35 *in situ* sampling stations were used for the development and re-parameterisation of the phytoplankton size model. We note that the remaining 35 sampling stations are representative of samples acquired at multiple depths (up to 20 metres). Thus, a total of 89 samples (corresponding to the remaining 35 stations) were used for the model re-parameterisation.

We utilised three different empirical, satellite ocean-colour algorithms in our analysis: the standard OC-CCI algorithm (which is a blended combination of the OC5 (*Gohin et al. 2002*) and the OC4v6 – OCI (*Hu et al. 2012*) algorithms) and the OC4 and OCI algorithms (*Hu et al. 2012; O'Reilly et al. 2000*) that have been regionally tuned for the Red Sea by *Brewin et al.* (*2015a*) (hereafter referred to as OC4-RG and OCI-RG respectively, Fig. 2). For further illustrative and qualitative validation of the

phytoplankton size model, daily images of satellite-derived phytoplankton size fractions from the OC-CCI product were also extracted for periods coinciding with the timing of *in situ* sample collection during the cruise programs (Table 1).

In addition, to provide an example highlighting the potential of new remote-sensing technologies and their application for mapping PSCs, we used a Chl-a dataset acquired from the Ocean and Land Colour Instrument (OLCI) on-board the recently launched Sentinel-3a satellite of the European Space Agency. An 8-day composite image for the period 28$^{th}$ February 2017 - 7$^{th}$ March 2017 was downloaded from the European Space Agency Copernicus Open Access Hub (https://scihub.copernicus.eu/). This dataset has a spatial resolution of 300 metres and was processed for the Red Sea using the regionally tuned algorithm developed by *Brewin et al*. (2015a).

### *2.5 Two-component phytoplankton size class model*

Following *Brewin et al*. (2015a), we used a two-component size class model to characterise the pico-phytoplankton and combined nano/micro-phytoplankton assemblages in the Red Sea. The model assumes small phytoplankton cells (picophytoplankton) are incapable of growing beyond a specific Chl-a concentration, and the addition of extra Chl-a into the system beyond this concentration can be attributed to the addition of larger phytoplankton cells (*Chisholm*, 1992; *Raimbault et al*. 1988). The model is based on the exponential equation originally put forth by *Sathyendranath et al.* (2001) and used by *Brewin et al.* (2010) to relate the concentration of Chl-a in pico-phytoplankton ($C_p$, cells < 2 μm) to the total Chl-a according to

$$C_p = C_p^m \left[1 - exp\left(-\frac{D_p}{C_p^m} C\right)\right] \quad (6).$$

The parameter $C_p{}^m$ represents the asymptotic maximum value of Chl-a associated with the pico-phytoplankton size class, whilst $D_p$ determines the fraction of total Chl-a for the picophytoplankton assemblage as total Chl-a ($C$) tends to zero. The size-specific Chl-a concentration of the combined nano/micro-phytoplankton assemblage ($C_{n,m}$) can subsequently be derived according to

$$C_{n,m} = C - C_p \quad (7).$$

The model parameters $C_p{}^m$ and $D_p$ were estimated by fitting Eq. 6 to the parameters $C_p$ and $C$, which were computed using the HPLC dataset. We used a non-linear, least squares fitting procedure (Trust-Region-Reflective algorithm, MATLAB Optimisation Toolbox, function 'LSQCURVEFIT'), in conjunction with bootstrapping (*Efron*, 1979), to compute the model parameters and their associated uncertainties (Table 3). Bootstrapping was implemented by randomly sub-sampling the dataset (1000 iterations) and re-fitting Eq. 6 for each sub-sample. The median and 95% confidence intervals were then computed from the resulting parameter distribution. The parameter $D_p$ was constrained to be less than or equal to 1, as size-fractionated Chl-a cannot exceed the total Chl-a concentration. The model parameters are presented in Table 3 and generally appear to lie within the range of values that have been computed for different regions of the global oceans.

**Table 3.** Model parameters derived from Equation 6 and comparisons with different studies.

| Study | Model Parameters | | Location | N | Method |
|---|---|---|---|---|---|
| | $C_p^m$ (mg $m^{-3}$) | $D_p$ | | | |
| *This study* | 0.19 (0.16 – 0.23) | 0.92 (0.85 - 1.0) | Red Sea | 89 | HPLC |
| *Brewin et al. (2012a)* | 0.17 | 0.82 | Indian Ocean | 686 | HPLC |
| *Brewin et al. (2011)* | 0.15 | 0.75 | Global | 256 | HPLC |
| *Brewin et al. (2015b)* | 0.13 (0.12 - 0.14) | 0.80 (0.78 - 0.82) | Global | 5841 | HPLC |
| *Brewin et al. (2010)* | 0.11 | 0.73 | Atlantic Ocean | 1935 | HPLC |
| *Brotas et al. (2013)* | 0.06 | 0.99 | NE Atlantic Ocean | 1100 | HPLC |
| *Brewin et al. (2017a)* | 0.13 (0.12 - 0.13) | 0.73 (0.71 - 0.76) | N Atlantic Ocean | 2239 | HPLC/SFF |

*2.6 Statistical tests*

For the assessment of satellite ocean-colour data and the validation of the re-parameterised model, we primarily used the Pearson linear correlation coefficient (r), mean absolute difference (MAD (M)) and bias (δ) as performance metrics to compare *in situ* and modelled values of total Chl-a, size fractions and size-specific Chl-a. The MAD is suggested to be less sensitive to different dataset distributions and the presence of outliers, and provides a natural and unambiguous characterisation of model uncertainty (*Willmott and Matsuura*, 2005). The MAD has been extensively utilised in other studies that involve comparisons between *in situ* and satellite estimates of chlorophyll (e.g. *Moses et al*. 2012; *O'Reilly and Werdell*, 2019) and phytoplankton size structure (e.g. *Brewin et al.* 2012a; *Corredor-Acosta et al.* 2018). The root-mean-square-difference (RMSD, ψ) is also presented in order to allow comparisons of the model performance with previous studies. We note that the linear correlation coefficient and RMSD have

previously been utilised to compare *in situ* and modelled data (*Brewin et al*. 2015c, 2016; *Doney et al*. 2009; *Friedrichs et al*. 2009). Statistical tests based on Chl-a concentrations were conducted in $\log_{10}$ space, as Chl-a tends to be log-normally distributed in the open ocean (*Campbell*, 1995). The MAD (M) was computed according to

$$M = \frac{\sum_{i=1}^{N} |X_i^E - X_i^M|}{N} \quad (8),$$

where N is the number of data points, X is the variable (total Chl-a concentration, size fraction or size-specific Chl-a) and the superscripts E and M correspond to the estimated variable from the model and the measured variable, respectively. The value of δ was calculated according to

$$\delta = \frac{1}{N}\left[\sum_{i=1}^{N} (X_i^E - X_i^M)\right] \quad (9)$$

and ψ was expressed as

$$\psi = \left[\frac{1}{N}\sum_{i=1}^{N} (X_i^E - X_i^M)^2\right]^{1/2} \quad (10).$$

## 3. RESULTS AND DISCUSSION

### *3.1 Satellite validation of total Chl-a*

To determine the best input of Chl-a for the phytoplankton size model, we first evaluate the performance of three different ocean colour algorithms (Fig. 2, Table 4). Irrespective of the type of algorithm, *in situ* values of Chl-a concentration are in good agreement with the satellite matchups and the relationships are characterised by high correlation coefficients ($r > 0.88$) and low mean absolute differences ($M < 0.2$). Using the correlation coefficient and RMSD ($\psi$) as a basis for comparison with previous studies, the model performance is similar, or in some cases better, to what has been previously observed in the Red Sea (*Brewin et al*. 2013, 2015a; *Racault et al*. 2015) and other regions of the global ocean (e.g. *Bailey and Werdell*, 2006; *Brewin et al*. 2015b; *Siegel et al*. 2013) (Table 4).

**Table 4.** Statistical results for the three ocean colour algorithms used in this study, and some comparisons with previous studies

| Study | Satellite dataset | Algorithm | r | Ψ | M | N | Region |
|---|---|---|---|---|---|---|---|
| *This study* | OC-CCI V3.1 | OC5/OC4v6-OCI | 0.88 | 0.14 | 0.12 | 14 | Red Sea |
| *This study* | OC-CCI V3.1 | OCI-RG | 0.89 | 0.22 | 0.19 | 14 | Red Sea |
| *This study* | OC-CCI V3.1 | OC4-RG | 0.88 | 0.17 | 0.13 | 14 | Red Sea |
| *Brewin et al. (2013)* | MODIS-Aqua | OC3 | 0.69 | 0.2 | - | 85 | Red Sea |
| *Brewin et al. (2013)* | MODIS-Aqua | OCI | 0.56 | 0.13 | - | 85 | Red Sea |
| *Brewin et al. (2015a)* | OC-CCI V1 | OCI-RG | 0.87 | 0.16 | - | 410 | Red Sea |
| *Brewin et al. (2015a)* | OC-CCI V1 | OC4-RG | 0.83 | 0.17 | - | 410 | Red Sea |
| *Racault et al*. (2015) | OC-CCI V1 | OC4 | 0.84 | 0.29 | - | 392 | Red Sea |
| *Brewin et al. (2012a)* | SeaWiFS | OC4 | 0.89 | - | 0.06 | 26 | Indian Ocean |
| *Lamont et al. (2018)* | MODIS-Aqua | OCI | 0.98 | 0.14 | - | 33 | Southern Africa |
| *Bailey and Werdell (2006)* | SeaWiFS | OC4 | 0.91 | 0.41 | - | 271 | Global |
| *Siegel et al. (2013)* | SeaWiFS | GSM | 0.88 | 0.36 | - | 1380 | Global |
| *Siegel et al. (2013)* | SeaWiFS | OC4 | 0.89 | 0.31 | - | 1543 | Global |
| *Brewin et al*. (2015b) | OC-CCI V1 | OC4 | 0.88 | 0.25 | - | 598 | Global |

Although the three algorithms exhibit a statistically similar performance (e.g. statistically similar values for the MAD (M) and RMSD (ψ) (95% confidence intervals overlap) and a statistically similar correlation coefficient (z-test)), the standard OC-CCI algorithm overestimates Chl-a concentration (δ = 0.08). This is analogous with the results of *Brewin et al*. (2015a) who found that the standard NASA OC4 and OCI algorithms

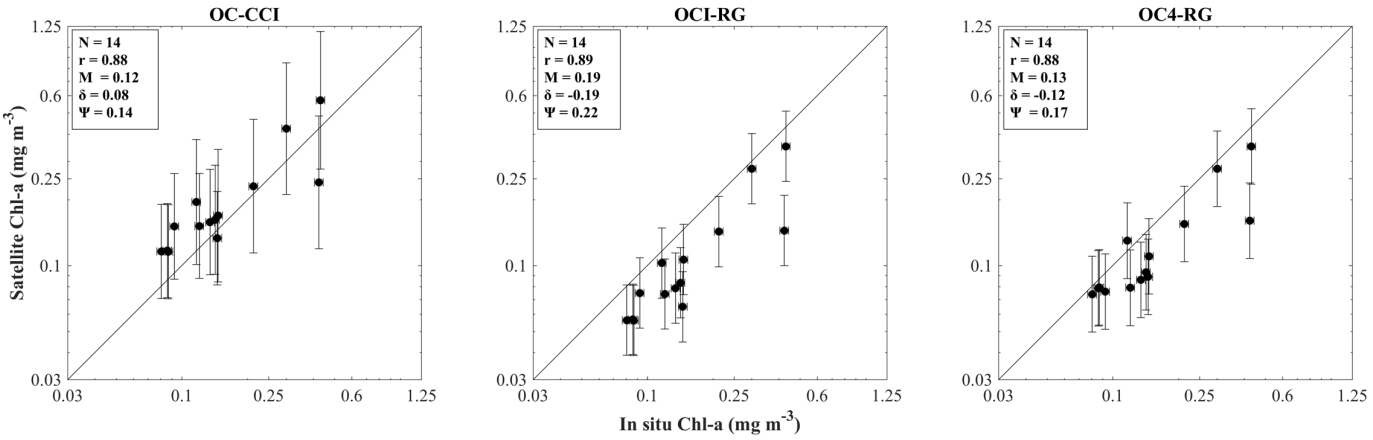


**Figure 2**. Satellite validation of total Chl-a concentration from three different empirical ocean colour algorithms; the standard OC-CCI algorithm and the regionally tuned OCI-RG and OC4-RG algorithms developed by *Brewin et al.* [2015a]. r is the Pearson correlation coefficient, M is the mean absolute difference, δ is the bias and ψ is the root-mean-square-difference. Statistical tests were computed in $\log_{10}$ space. Per-pixel uncertainties for the matchups obtained using the standard OC-CCI algorithm are provided as RMSD error bars. Overall, the *in situ* Chl-a matchups are within the uncertainty limits of the OC-CCI data. We also present the fixed RMSD uncertainties for OCI-RG and OC4-RG, which are based on a previous validation of those algorithms using OC-CCI data (see Fig 7 of *Brewin et al. 2015a*). Uncertainties associated with *in*

417 *situ* Chl-a concentrations are expressed as percentages (~ +/- 4.6%) and are represented
418 by the black horizontal error bars.
419
420 systematically overestimate Chl-a in the Red Sea. They attributed this overestimation to
421 increased chromophoric dissolved organic matter (CDOM) absorption per unit Chl-a.
422 This hypothesis was recently corroborated by *Kheireddine et al*. (2018b), who analysed
423 the spatial distribution of the absorption coefficient of CDOM ($a_{CDOM}$), using *in situ*
424 measurements acquired during several cruises conducted in the Red Sea. *Kheireddine et*
425 *al*. (2018b) observed that values of $a_{CDOM}$ for a specific Chl-a concentration were
426 substantially higher in the Red Sea in comparison to the adjacent Mediterranean Sea (20 -
427 550%) (*Organelli et al*. 2014). The authors also revealed that CDOM concentrations were
428 higher than what has been observed in other oligotrophic regions, such as the southeast
429 Pacific and Mediterranean Sea (*Bricaud et al*. 2010; *Morel and Gentili*, 2009).
430 The regionally tuned OCI-RG and OC4-RG algorithms are associated with
431 negative biases ($\delta$ = -0.19 and -0.12 respectively), particularly the OCI-RG algorithm,
432 which displays a consistent underestimation of Chl-a (Fig. 2). However, considering the
433 improved performance of the regionally-tuned Red Sea algorithms previously obtained
434 using a larger match-up dataset (*Brewin et al*. 2015a), and it's slightly higher statistical
435 performance in comparison to OCI-RG, we opted to use the OC4-RG algorithm for input
436 to the PSC model. On-going research is required to monitor the performance of all these
437 algorithms, as and when more data become available in the Red Sea.
438
439

*3.2 Re-parameterisation of the two-component phytoplankton size model*

The re-parameterised size model was fitted to the Red Sea HPLC dataset (Fig. 3, black line), and for comparison, was plotted alongside the previous two-component model of *Brewin et al*. (2015a) (Fig. 3, red line). Overall, the re-parameterised model adequately captures the general trends in *in situ* derived size-specific Chl-a ($C_p$, $C_{n,m}$) as a function of total Chl-a ($r > 0.9$, $M < 0.1$). The contribution of Chl-a from the pico-phytoplankton assemblage is higher at low Chl-a concentrations and the model parameter $D_p$ is representative of the increase in pico-phytoplankton as the total Chl-a concentration tends to zero ($D_p = 0.92$). Above an asymptotic Chl-a concentration of ~ 0.19 mg $m^{-3}$ for pico-phytoplankton ($C_p$), additional Chl-a in the system can be attributed to increases in Chl-a within the nano/micro- phytoplankton assemblage ($C_{n,m}$). The model also captures the general trends observed for the phytoplankton size fractions ($F_p$, $F_{n,m}$), where the fraction of small (larger) cells decreases (increases) with the total Chl-a concentration.

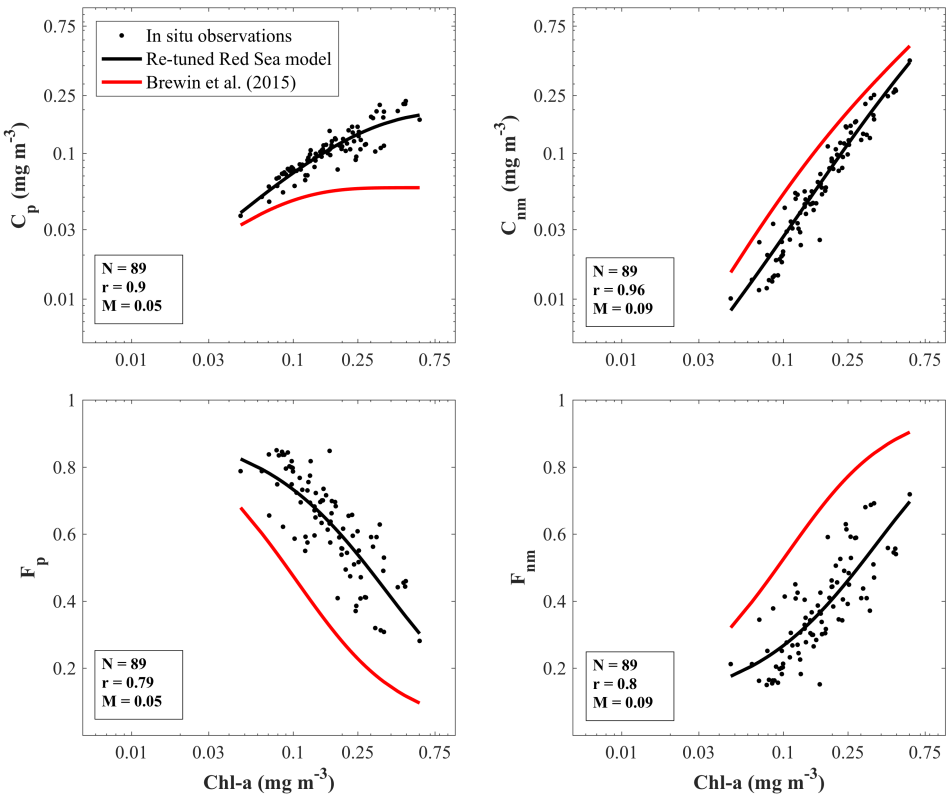


**Figure 3.** The two-component phytoplankton size model fitted alongside the Red Sea HPLC pigment data. The black and red lines represent the re-parameterised model and the original model of *Brewin et al.* (2015a) respectively. The top row shows the relationship between total Chl-a concentration and size-specific Chl-a, whilst the bottom row shows the relationship between total Chl-a and the fraction of total Chl-a from the two size classes.

Although the model of *Brewin et al.* (2015a) displays the same general trend, it underestimates $C_p$ and $F_p$, and overestimates $C_{n,m}$ and $F_{n,m}$, for a given total Chl-a concentration (Fig. 3). We note that these differences are apparent regardless of the choice of regression coefficients for Eq. 2 (Supplementary Fig. 2). Prior to the re-tuning

of the size model, *Brewin et al*. (2015a) had set the value of the model parameter $C_p^m$ (the maximum Chl-a concentration reached by the pico-phytoplankton population) at 0.06 mg $m^{-3}$ (Table 3). Considering the updated model parameter in this study ($C_p^m$ = 0.19 mg $m^{-3}$), the previous value of $C_p^m$ utilised by *Brewin et al*. (2015a), which was derived using HPLC datasets collected in the eastern North Atlantic Ocean (see *Brotas et al*. 2013), probably under-represents the contribution of the pico-phytoplankton population. Indeed, *Brewin et al*. (2015a) and *Kheireddine et al*. (2017) revealed that pico-phytoplankton constituted the dominant size class in the Red Sea, although in the case of the latter study, community structure was found to be fairly heterogeneous due to the mesoscale variability of the region.

*3.3 Satellite validation of size-specific Chl-a concentrations and size fractions*

Satellite-derived observations of Chl-a concentration from the independent matchup dataset were used as input to the re-parameterised two-component size class model, and accordingly, size-specific Chl-a and size fractions were derived. The resultant relationships between the satellite and *in situ* data are presented in Figure 4. Generally, satellite estimates of size-specific Chl-a concentration match the *in situ* observations well. For both $C_p$ and $C_{n,m}$, high r values ($r > 0.80$) and low MAD ($M < 0.2$) are obtained. A slight negative bias occurs for both size classes (-0.11), which is most likely related to the underestimation of total Chl-a from the OC4-RG algorithm (Fig. 2). To further assess the performance of the re-parameterised model, we present the results of statistical tests computed for matchups obtained using the previous model parameters of *Brewin et al*.

509 (2015a) (Fig. 4). Overall, following model re-parameterisation, the bias is closer to zero,
510 the MAD is smaller and the RMSD is approximately halved (excluding the RMSD
511 associated with the size-specific Chl-a concentration of the combined nano-micro
512 assemblage [$C_{n,m}$]). In addition, the RMSD of $C_p$ presented here ($\psi = 0.13$) is lower than
513 what has been observed in the global ocean (*Brewin et al*. 2015b), the North Atlantic
514 (*Brewin et al*. 2017a) the waters off Central-Southern Chile (*Corredor-Acosta et al*.
515 2018) and South Africa (*Lamont et al*. 2018). Satellite-derived size fractions ($F_p$ and $F_{n,m}$)
516 are also in good agreement with the *in situ* observations ($r = 0.67$) and the relationships
517 are characterised by low MAD ($M = 0.09$) and low biases ($\delta = \pm 0.02$). We note that as
518 $F_{n,m} = 1 - F_p$ (see Eq. 3), the statistical parameters computed for the matchups of $F_p$ and
519 $F_{n,m}$ are identical (although characterised by a change of sign for the case of $\delta$).
520 To investigate spatial gradients in satellite estimates of phytoplankton size
521 structure, we present an 8-day composite image of the pico- and nano/micro-
522 phytoplankton fractions in the CRS region, as well as total Chl-a concentration (Fig. 5).
523 The composite image represents the period 1st - 9th April 2015, corresponding
524 approximately to the sampling dates of the NC2 cruise conducted in the CRS (3rd – 9th
525 April 2015, Table 1). For comparison, the *in situ* size fractions of the pico- and
526 nano/micro- phytoplankton assemblage from the NC2 sampling stations are overlaid on
527 the satellite image (Fig. 5, white circles).
528
529
530
531

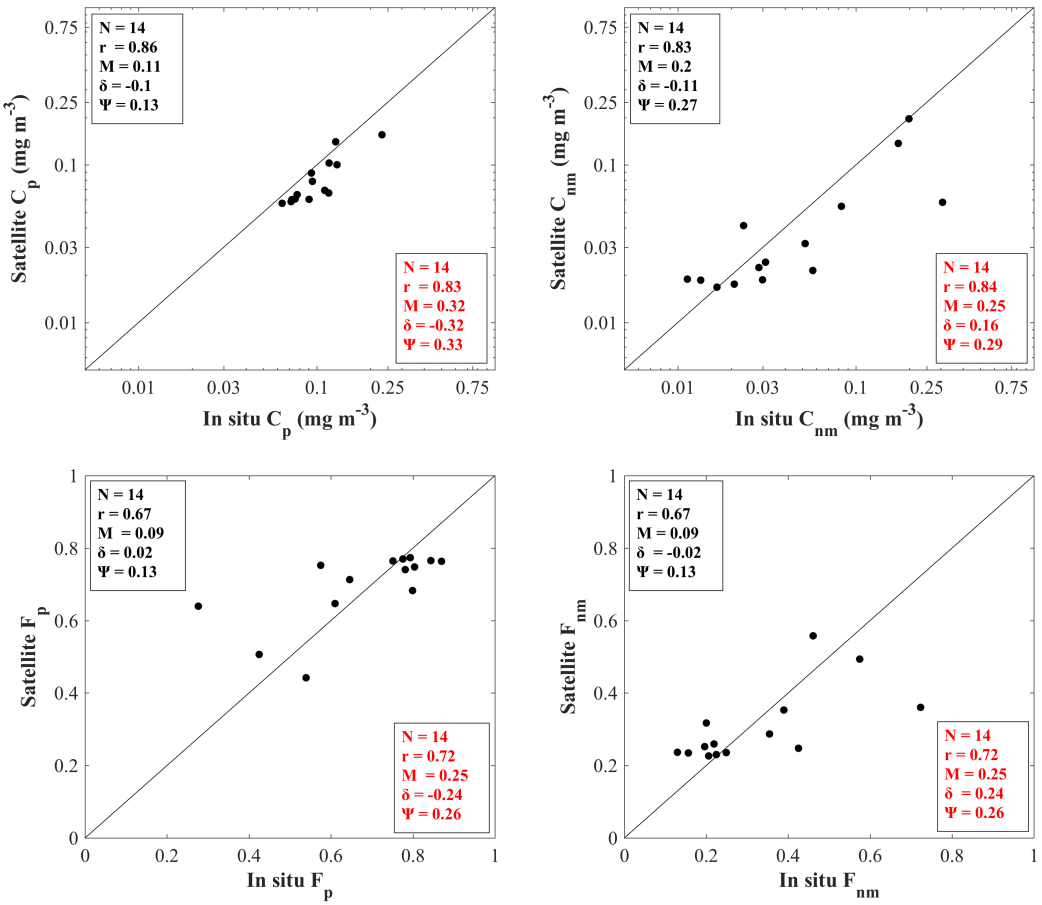


**Figure 4.** Satellite validation of size-specific Chl-a concentrations (top row) and the fractional contribution of Chl-a to total Chl-a (bottom row) for the two size classes. Statistical tests were computed in $\log_{10}$ space for size-specific Chl-a concentrations and in linear space for the size fractions. The statistical parameters are the same as those described in Figure 2. For comparison, statistical tests are also presented (in red text) for matchups computed using the previous Red Sea model parameterisation of *Brewin et al.* (2015a).

The satellite data effectively capture the spatial variability of *in situ* size fractions. Lower fractions of nano/micro- phytoplankton (~ 20 - 25% of the total population) are

apparent in the northern region of the CRS (22 – 24°N), coinciding with reduced Chl-a concentrations and a higher fraction of pico-phytoplankton (75 – 80%). The fraction of nano/micro- phytoplankton increases to ~ 35% between 21 and 22°N, and this is observed by the most southerly *in situ* sampling station at ~ 21.75°N. This region of larger cells is characterised by higher Chl-a concentrations and extends from the eastern coast towards the western coastline. We speculate that this feature may be representative of a mesoscale anticylonic eddy that is a capable of transporting water masses across the basin. Large eddies are known to occur frequently in the CRS (~ 18 – 24°N) (*Zhan et al*. 2014, 2019) and previous research has demonstrated how these eddies transfer waters rich in Chl-a between the east and west coastlines of the Red Sea (*Raitsos et al*. 2017). Coral reefs contain elevated concentrations of nutrients from processes such as grazing, sediment re-suspension and bacterial respiration (*Acker et al*. 2008; *Erez*, 1990; *Rasheed et al*. 2002) and instances of higher nutrient availability are known to correlate with larger phytoplankton cells (*Marañón*, 2015). Indeed, total Chl-a concentration and the fraction of larger cells is notably higher along the coastlines of the CRS, constituting 40 – 60% of the total phytoplankton population. The eddy may advect larger cells further offshore between 21 and 22°N at its periphery, whilst simultaneously driving a decrease in total Chl-a concentration, and an increase in the contribution of pico-phytoplankton at its core (~ 22.5°N), as a result of downwelling and enhanced oligotrophy.

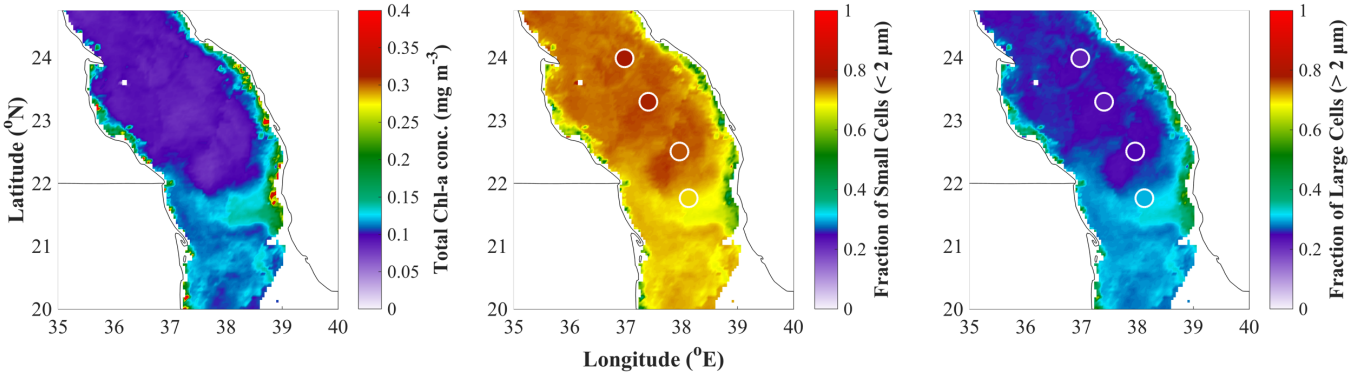


**Figure 5.** 8-day climatology (1st – 9th April 2015) of total Chl-a (computed using the OC4-RG algorithm), and the fractional contributions of pico- and the combined nano/micro- phytoplankton assemblages generated using the updated model parameters. *In situ* data points from the NC2 cruise, conducted during this 8-day period (Table 1), are overlaid on the satellite imagery and are represented by the white circles. The *in situ* samples are plotted with the same colour scale as the satellite image.

### *3.4 Potential caveats*

#### *3.4.1 In situ estimates of phytoplankton size structure*

We utilised a Red Sea HPLC dataset, in conjunction with a diagnostic pigment approach, to derive *in situ* measurements of size-specific Chl-a concentration that would be used for the re-parameterisation of the two-component size class model of Brewin et al (2015a). We note that some diagnostic pigments may be shared by several phytoplankton groups that span a broad range of sizes, and thus may not always be precise biomarkers that enable the definitive differentiation between size classes. In consideration of this,

601 refinements have been made to infer size fractionated Chl-a from the HPLC data using
602 the diagnostic pigment approach. Specifically, we followed the approach of *Brewin et al*.
603 (2010) to compute *in situ* values of the pico-phytoplankton size fraction ($F_p$). This
604 involved apportioning some of the 19′-hexanoyloxyfucoxanthin pigment to pico-
605 phytoplankton at lower Chl-a concentrations, as some pico-eukaryotes contain this
606 pigment. Considering that a two-component model was used to derive pico-
607 phytoplankton and the combined nano/micro-phytoplankton assemblages, it was not
608 necessary to implement further adjustments that have been previously used to account for
609 the partitioning of pigments between micro-phytoplankton and nano-phytoplankton (e.g.
610 *Devred et al*. 2011). Although we did not compare HPLC-derived estimates of size-
611 fractioned Chl-a with those derived using other methods (e.g. size-fractionated filtration,
612 flow cytometry or molecular analysis), systematic differences in size-fractionated Chl-a
613 between HPLC and other methods have been observed (e.g. *Brewin et al.* 2014a). Future
614 efforts should focus on collecting concurrent data on size-fractioned Chl-a in the Red Sea
615 using multiple methods, for a more complete and accurate diagnosis of phytoplankton
616 size classes (*Nair et al*. 2008). Until such datasets become available, the HPLC approach
617 is our only *in situ* resource, and it has been shown to capture trends in phytoplankton size
618 structure in other oceanic regions (*Organelli et al*. 2013; *Uitz et al*. 2008, 2015).
619 Furthermore, the conceptual framework of the two-component model used here has been
620 supported by multiple *in situ* methods, including: size-fractionated filtration
621 measurements (*Brewin et al.,* 2014b; *Gin et al.,* 2000; *Marañón et al.,* 2012;),
622 measurements from flow cytometry and microscopy (*Brotas et al.*, 2013), and

623 measurements of spectral absorption by phytoplankton and particle backscattering
624 (*Brewin et al.,* 2011, *Brewin et al.,* 2012b; *Devred et al.,* 2006, 2011).
625
626 *3.4.2 Abundance-based phytoplankton size model*
627
628 The abundance-based, three-component model conceptualised by *Brewin et al*. (2010),
629 and adapted for the Red Sea by *Brewin et al.* (2015a), has been applied and validated
630 both globally, and for individual oceanic regions (e.g. *Brewin et al.* 2010, 2012a, 2014a,
631 2015a, 2015b; *Hu et al*. 2018; *Lamont et al*. 2018; *Lin et al*. 2014). However, abundance-
632 based algorithms infer phytoplankton size structure based on relationships between the
633 total Chl-a concentration and size-fractionated Chl-a, and thus do not directly detect the
634 presence of different phytoplankton size classes. Although these relationships have been
635 shown to hold across the global oceans, deviations from these relationships occur (e.g.
636 *Goericke*, 2011). Furthermore, for applications of the model to satellite data in optically-
637 complex waters, satellite retrievals of Chl-a may be impacted by the presence of CDOM
638 and non-algal particles (*Hirata et al*. 2011; *Mouw et al*. 2017). Modifications to
639 ecosystem structure as a result of climate change may alter relationships between
640 phytoplankton size structure and total Chl-a (*Agirbas et al.* 2015; *Racault et al.* 2014;
641 *Sathyendranath et al.* 2017). Thus, as well as a need for increased *in situ* sampling efforts
642 in the Red Sea, re-calibration of abundance-based algorithms may be necessary in the
643 future, and may require tying model parameters ($C_p^m$ and $D_p$) to other environmental
644 variables amenable from space (see *Brewin et al.* 2015b, 2017a; *Ward,* 2015).

Abundance-based algorithms use total Chl-a from satellite remote sensing as input. Thus, the accuracy of satellite Chl-a observations is critical for the derivation of accurate size-fractionated Chl-a data. Per-pixel uncertainties in satellite size-fractionated Chl-a data can be derived in two ways: 1) by propagating errors in the input total Chl-a through to the output size-fractionated Chl-a, accounting for uncertainties in model parameters (*Brewin et al.* 2017b); or 2) through comparison of satellite size-fractionated Chl-a with *in situ* data (validation), by matching the two estimates in time and space (*Brewin et al.* 2017a). Each approach has its advantages and disadvantages. Model error propagation requires good knowledge of errors in model parameters and model input, and assumes the model is conceptually accurate. Validation generally assumes the *in situ* data are correct, when in reality the *in situ* measurements have their own uncertainties that should be considered in the analysis, but are difficult to estimate (*Brewin et al*. 2014b, 2017a; *Nair et al*. 2008). In addition, when comparing satellite data with concurrent *in situ* data, the scales of the observations differ by orders of magnitude (e.g. 1 litre HPLC sample and 4km satellite pixel), which can cause additional uncertainties. In our study we report the uncertainties based on validation (see Figure 4). It is envisaged that future work could improve on this, perhaps making use of optical water type classification methods (e.g. *Brewin et al*. 2017a), and by characterising uncertainties in the *in situ* data, through the collection of concurrent *in situ* size-fractioned Chl-a data using multiple methods.

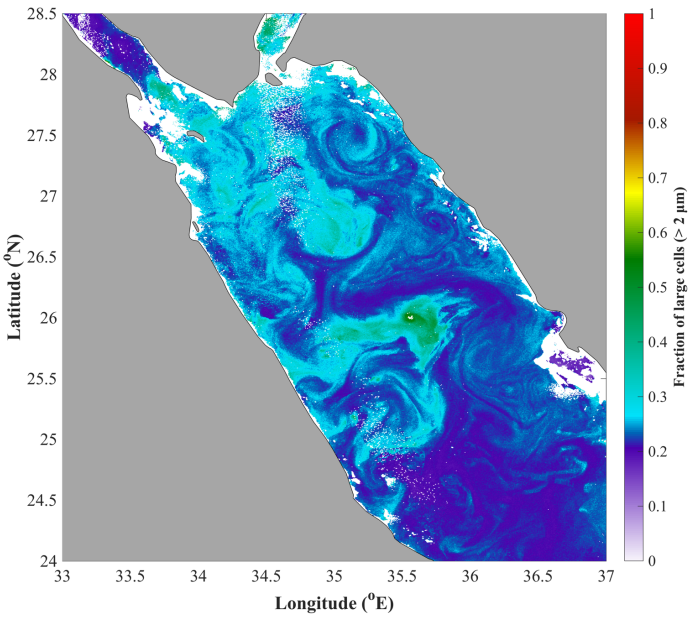


**Figure 6.** 8-day climatology (28th February – 7th March 2017) showing the fractional contribution of the combined nano/micro- phytoplankton assemblage at a spatial resolution of 300 metres. The size fraction was computed using parameters from the re-parameterised model and observations of Chl-a concentration acquired via the Ocean and Land Colour Instrument (OLCI) on-board the SENTINEL-3 satellite (European Space Agency).

## 4. CONCLUSIONS

We re-parameterised the two-component phytoplankton size model of *Brewin et al.* (2015a) using HPLC pigment data collected in the Red Sea. The updated model effectively captures the relationships between *in situ* measurements of total Chl-a concentration and the Chl-a concentrations of the pico- and combined nano/micro-phytoplankton size classes, and was subsequently applied to remotely-sensed ocean

colour observations. Overall, satellite estimates of phytoplankton size structure correlate well with concurrent *in situ* measurements and also capture the spatial variability in phytoplankton size structure related to an anticyclonic eddy.

To our knowledge, this analysis provides the first *in situ* validation of satellite-derived estimates of phytoplankton size structure in the Red Sea and paves the way for further investigation on the seasonality, interannual variability and phenology of different PSCs. This is likely to be paramount for developing a better understanding of trophic relationships and fisheries dynamics in the region, contributing to the development and implementation of marine ecosystem management schemes. Finally, with the advent of more advanced remote-sensing capabilities, including the launch of next-generation satellite sensors such as OLCI on-board the Sentinel-3a spacecraft (European Space Agency), the large-scale spatiotemporal distribution of ecological indicators, as well as their linkages to mesoscale variability, can be resolved at much finer temporal scales (Fig. 6).

714 **5. REFERENCES**

715

716 Acker, J., Leptoukh, G., Shen, S., Zhu, T., Kempler, S., 2008. Remotely-sensed
717 chlorophyll a observations of the northern Red Sea indicate seasonal variability and
718 influence of coastal reefs. J. Mar. Syst. 69, 191–204.
719 https://doi.org/10.1016/j.jmarsys.2005.12.006.

720

721 Agirbas, E., Martinez-Vicente, V., Brewin, R.J., Racault, M.F., Airs, R.L. and Llewellyn,
722 C.A., 2015. Temporal changes in total and size-fractioned chlorophyll-a in surface waters
723 of three provinces in the Atlantic Ocean (September to November) between 2003 and
724 2010. J. Mar. Syst. 150, 56-65. https://doi.org/10.1016/j.jmarsys.2015.05.008.

725

726 Al-Najjar, T., Badran, M. I., Richter, C., Meyerhoefer, M., Sommer, U., 2007. Seasonal
727 dynamics of phytoplankton in the Gulf of Aqaba, Red Sea. Hydrobiologia 579(1), 69-83.
728 http://dx.doi.org/10.1007/s10750-006-0365-z.

729

730 Bailey, S.W., Werdell, P.J., 2006. A multi-sensor approach for the on-orbit validation of
731 ocean color satellite data products. Remote Sens. Environ. 102, 12–23.
732 https://doi.org/10.1016/J.RSE.2006.01.015.

733

734 Berumen, M. L., Hoey, A. S., Bass, W. H., Bouwmeester, J., Catania, D., Cochran, J. E.
735 M., Khalil, M. T., Miyake, S., Mughal, M. R., Spaet, J. L. Y., Saenz-Agudelo, P., 2013.

736 The status of coral reef ecology research in the Red Sea. Coral Reefs 32(3), 737–748.
737 http://doi.org/10.1007/s00338-013-1055-8.
738
739 Boyd, P. W., Newton, P., 1999. Does planktonic community structure determine
740 downward particulate organic carbon flux in different oceanic provinces? Deep Sea Res.
741 Part I. 46, 63–91. doi:10.1016/S0967-0637(98)00066-1.
742
743 Bracher, A., Bouman, H.A., Brewin, R.J., Bricaud, A., Brotas, V., Ciotti, A.M.,
744 Clementson, L., Devred, E., Di Cicco, A., Dutkiewicz, S., Hardman-Mountford, N.J.,
745 2017. Obtaining phytoplankton diversity from ocean color: a scientific roadmap for
746 future development. Front. Mar. Sci. 4, 55. https://doi.org/10.3389/fmars.2017.00055.
747
748 Brewin, R.J.W., Ciavatta, S., Sathyendranath, S., Jackson, T., Tilstone, G., Curran, K.,
749 Airs, R.L., Cummings, D., Brotas, V., Organelli, E., Dall'Olmo, G., Raitsos, D.E., 2017a.
750 Uncertainty in Ocean-Color Estimates of Chlorophyll for Phytoplankton Groups. Front.
751 Mar. Sci. 4, 104. https://doi.org/10.3389/fmars.2017.00104.
752
753 Brewin, R.J.W., Dall'Olmo, G., Pardo, S., van Dongen-Vogels, V., Boss, E.S., 2016.
754 Underway spectrophotometry along the Atlantic Meridional Transect reveals high
755 performance in satellite chlorophyll retrievals. Remote Sens. Environ. 183, 82–97.
756 https://doi.org/10.1016/j.rse.2016.05.005.
757

Brewin, R.J.W., Dall'Olmo, G., Sathyendranath, S., Hardman-Mountford, N.J., 2012b. Particle backscattering as a function of chlorophyll and phytoplankton size structure in the open-ocean. Opt. Express 20, 17632. https://doi.org/10.1364/OE.20.017632.

Brewin, R.J.W., Devred, E., Sathyendranath, S., Lavender, S.J., Hardman-Mountford, N.J., 2011. Model of phytoplankton absorption based on three size classes. Appl. Opt. 50, 4535. https://doi.org/10.1364/AO.50.004535.

Brewin, R.J.W., Hirata, T., Hardman-Mountford, N.J., Lavender, S.J., Sathyendranath, S., Barlow, R., 2012a. The influence of the Indian Ocean Dipole on interannual variations in phytoplankton size structure as revealed by Earth Observation. Deep. Res. Part II Top. Stud. Oceanogr. 77–80, 117–127. https://doi.org/10.1016/j.dsr2.2012.04.009.

Brewin, R.J.W., Jackson, T., Cain, T., Miller, P.I., Lange, P.K., Misra, A., Airs, R.L., 2017b. Modelling size-fractionated primary production in the Atlantic Ocean from remote sensing. Prog. Oceanogr. 158, 130–149. https://doi.org/10.1016/J.POCEAN.2017.02.002.

Brewin, R.J.W., Raitsos, D.E., Dall'Olmo, G., Zarokanellos, N., Jackson, T., Racault, M.F., Boss, E.S., Sathyendranath, S., Jones, B.H., Hoteit, I., 2015a. Regional ocean-colour chlorophyll algorithms for the Red Sea. Remote Sens. Environ. 165, 64–85. https://doi.org/10.1016/j.rse.2015.04.024.

781 Brewin, R.J.W., Raitsos, D.E., Pradhan, Y., Hoteit, I., 2013. Comparison of chlorophyll
782 in the Red Sea derived from MODIS-Aqua and in vivo fluorescence. Remote Sens.
783 Environ. 136, 218–224. https://doi.org/10.1016/J.RSE.2013.04.018.
784
785 Brewin, R.J.W., Sathyendranath, S., Hirata, T., Lavender, S.J., Barciela, R.M., Hardman-
786 Mountford, N.J., 2010. A three-component model of phytoplankton size class for the
787 Atlantic Ocean. Ecol. Modell. 221, 1472–1483.
788 https://doi.org/10.1016/j.ecolmodel.2010.02.014.
789
790 Brewin, R.J.W., Sathyendranath, S., Jackson, T., Barlow, R., Brotas, V., Airs, R.,
791 Lamont, T., 2015b. Influence of light in the mixed-layer on the parameters of a three-
792 component model of phytoplankton size class. Remote Sens. Environ. 168, 437–450.
793 https://doi.org/10.1016/j.rse.2015.07.004.
794
795 Brewin, R.J.W., Sathyendranath, S., Lange, P.K., Tilstone, G., 2014a. Comparison of two
796 methods to derive the size-structure of natural populations of phytoplankton. Deep Sea
797 Res. Part I Oceanogr. Res. Pap. 85, 72–79. https://doi.org/10.1016/J.DSR.2013.11.007.
798
799 Brewin, R.J.W., Sathyendranath, S., Müller, D., Brockmann, C., Deschamps, P.-Y.,
800 Devred, E., Doerffer, R., Fomferra, N., Franz, B., Grant, M., Groom, S., Horseman, A.,
801 Hu, C., Krasemann, H., Lee, Z., Maritorena, S., Mélin, F., Peters, M., Platt, T., Regner,
802 P., Smyth, T., Steinmetz, F., Swinton, J., Werdell, J., White, G.N., 2015c. The Ocean
803 Colour Climate Change Initiative: III. A round-robin comparison on in-water bio-optical

algorithms. Remote Sens. Environ. 162, 271–294. https://doi.org/10.1016/J.RSE.2013.09.016.

Brewin, R.J.W., Sathyendranath, S., Tilstone, G., Lange, P.K., Platt, T., 2014b. A multicomponent model of phytoplankton size structure. J. Geophys. Res. Ocean. 119, 3478–3496. https://doi.org/10.1002/2014JC009859.

Bricaud, A., Babin, M., Claustre, H., Ras, J., Tièche, F., 2010. Light absorption properties and absorption budget of Southeast Pacific waters. J. Geophys. Res. 115, C08009. https://doi.org/10.1029/2009JC005517.

Briggs, N., Perry, M. J. P., Cetinic´, I., Lee, C., D'Asaro, E., Gray, A. M., Rehm, E., 2011. High-resolution observations of aggregate flux during a sub-polar North Atlantic spring bloom, Deep Sea Res. Part I 58, 1031–1039. doi:10.1016/j.dsr.2011.07.007.

Brito, A.C., Sá, C., Brotas, V., Brewin, R.J., Silva, T., Vitorino, J., Platt, T., Sathyendranath, S., 2015. Effect of phytoplankton size classes on bio-optical properties of phytoplankton in the Western Iberian coast: Application of models. Remote Sens. Environ. 156, 537-550. https://doi.org/10.1016/j.rse.2014.10.020.

Brotas, V., Brewin, R.J.W., Sá, C., Brito, A.C., Silva, A., Mendes, C.R., Diniz, T., Kaufmann, M., Tarran, G., Groom, S.B., Platt, T., Sathyendranath, S., 2013. Deriving phytoplankton size classes from satellite data: Validation along a trophic gradient in the

827 eastern Atlantic Ocean. Remote Sens. Environ. 134, 66–77.
828 https://doi.org/10.1016/J.RSE.2013.02.013.
829
830 Campbell, J.W., 1995. The lognormal distribution as a model for bio-optical variability in
831 the sea. J. Geophys. Res. 100, 13237. https://doi.org/10.1029/95JC00458.
832
833 Cantin, N. E., Cohen, A. L., Karnauskas, K. B., Tarrant, A. M., McCorkle, D. C., 2010.
834 Ocean warming slows coral growth in the central Red Sea. Science 329(5989), 322-325.
835 https://doi.org/10.1126/science.1190182.
836
837 Carvalho, S., Kurten, B., Krokos, G., Hoteit, I., 2018. The Red Sea in: Sheppard, C.
838 (Eds.) Introduction to World Seas: An Environmental Evaluation 2nd Edition. Volume II:
839 The Indian Ocean to the Pacific. Academic Press.
840
841 Chaidez, V., Dreano, D., Agusti, S., Duarte, C.M., Hoteit, I., 2017. Decadal trends in Red
842 Sea maximum surface temperature. Sci. Rep. 1–8. https://doi.org/10.1038/s41598-017-
843 08146-z.
844
845 Chisholm, S. W. 1992. Phytoplankton size. In Primary productivity and biogeochemical
846 cycles in the sea. Springer, Boston, MA.
847

Claustre, H., 1994. The trophic status of various oceanic provinces as revealed by phytoplankton pigment signatures. Limnol. Oceanogr. 39(5), 1206-1210. https://doi.org/10.4319/lo.1994.39.5.1206.

Corredor-Acosta, A., Morales, C.E., Brewin, R.J.W., Auger, P.A., Pizarro, O., Hormazabal, S., Anabalón, V., 2018. Phytoplankton size structure in association with mesoscale Eddies off Central-Southern Chile: The satellite application of a phytoplankton size-class model. Remote Sens. 10. https://doi.org/10.3390/rs10060834.

Devred, E., Sathyendranath, S., Stuart, V., Maass, H., Ulloa, O., Platt, T., 2006. A two-component model of phytoplankton absorption in the open ocean : Theory and applications 111, 1–11. https://doi.org/10.1029/2005JC002880.

Devred, E., Sathyendranath, S., Stuart, V., Platt, T., 2011. A three component classification of phytoplankton absorption spectra : Application to ocean-color data. Remote Sens. Environ. 115(9), 2255–2266. https://doi.org/10.1016/j.rse.2011.04.025.

Doney, S.C., Lima, I., Moore, J.K., Lindsay, K., Behrenfeld, M.J., Westberry, T.K., Mahowald, N., Glover, D.M., Takahashi, T., 2009. Skill metrics for confronting global upper ocean ecosystem-biogeochemistry models against field and remote sensing data. J Mar. Syst. 76(1-2), 95-112. https://doi.org/10.1016/j.jmarsys.2008.05.015.

870 Dreano, D., Raitsos, D.E., Gittings, J., Krokos, G., Hoteit, I., 2016. The Gulf of Aden
871 Intermediate Water Intrusion Regulates the Southern Red Sea Summer Phytoplankton
872 Blooms. PLoS One 1–20. https://doi.org/10.1371/journal.pone.0168440.
873
874 Efron, B., 1979. Bootstrap methods: Another look at the jackknife, Ann. Stat. 7, 1–26.
875
876 Eppley, R. W., Peterson, B. J., 1979. Particulate organic matter flux and planktonic new
877 production in the deep ocean. Nature 282, 677–680. doi:10.1038/282677a0.
878
879 Erez, J., 1990. On the importance of food sources in coral-reef ecosystems. Ecosystems
880 of the world, 25, 411-418.
881
882 Friedrichs, M.A.M., Carr, M.-E., Barber, R.T., Scardi, M., Antoine, D., Armstrong, R.A.,
883 Asanuma, I., Behrenfeld, M.J., Buitenhuis, E.T., Chai, F., Christian, J.R., Ciotti, A.M.,
884 Doney, S.C., Dowell, M., Dunne, J., Gentili, B., Gregg, W., Hoepffner, N., Ishizaka, J.,
885 Kameda, T., Lima, I., Marra, J., Mélin, F., Moore, J.K., Morel, A., O'Malley, R.T.,
886 O'Reilly, J., Saba, V.S., Schmeltz, M., Smyth, T.J., Tjiputra, J., Waters, K., Westberry,
887 T.K., Winguth, A., 2009. Assessing the uncertainties of model estimates of primary
888 productivity in the tropical Pacific Ocean. J. Mar. Syst. 76, 113–133.
889 https://doi.org/10.1016/J.JMARSYS.2008.05.010.
890

Gin, K.Y.-H., Lin, X., Zhang, S., 2000. Dynamics and size structure of phytoplankton in the coastal waters of Singapore. J. Plankton Res. 22, 1465–1484. https://doi.org/10.1093/plankt/22.8.1465.

Gittings, J.A., Raitsos, D.E., Kheireddine, M., Racault, M.-F., Claustre, H., Hoteit, I., 2019. Evaluating tropical phytoplankton phenology metrics using contemporary tools. Sci. Rep. 9, 674. https://doi.org/10.1038/s41598-018-37370-4.

Gittings, J.A., Raitsos, D.E., Krokos, G., Hoteit, I., 2018. Impacts of warming on phytoplankton abundance and phenology in a typical tropical marine ecosystem. Sci. Rep. 8, 2240. https://doi.org/10.1038/s41598-018-20560-5.

Gittings, J.A., Raitsos, D.E., Racault, M., Brewin, R.J.W., Pradhan, Y., Sathyendranath, S., Platt, T., 2017. Remote Sensing of Environment Seasonal phytoplankton blooms in the Gulf of Aden revealed by remote sensing. Remote Sens. Environ. 189, 56–66. https://doi.org/10.1016/j.rse.2016.10.043.

Gladstone, W., Curley, B., Shokri, M. R., 2013. Environmental impacts of tourism in the Gulf and the Red Sea. Mar. Pollut. Bull. 72(2), 375–388. https://doi.org/10.1016/j.marpolbul.2012.09.017.

912 GoeRicke, R., 2011. The size structure of marine phytoplankton-what are the rules.
913 CalCOFI Rep, 52, 198-204.
914
915 Gohin, F., Druon, J.N., Lampert, L., 2002. A five channel chlorophyll concentration
916 algorithm applied to SeaWiFS data processed by SeaDAS in coastal waters. Int. J.
917 Remote Sens. 23, 1639–1661. https://doi.org/10.1080/01431160110071879.
918
919 Guidi, L., Stemmann, L., Jackson, G.A., Ibanez, F., Claustre, H., Legendre, L., Picheral,
920 M., Gorskya, G., 2009. Effects of phytoplankton community on production, size, and
921 export of large aggregates: A world-ocean analysis. Limnol. Oceanogr. 54, 1951–1963.
922 https://doi.org/10.4319/lo.2009.54.6.1951
923
924 Hirata, T., Hardman-Mountford, N.J., Brewin, R.J.W., Aiken, J., Barlow, R., Suzuki, K.,
925 Isada, T., Howell, E., Hashioka, T., Noguchi-Aita, M., Yamanaka, Y., 2011. Synoptic
926 relationships between surface Chlorophyll-a and diagnostic pigments specific to
927 phytoplankton functional types. Biogeosciences 8, 311–327. https://doi.org/10.5194/bg-
928 8-311-2011.
929
930 Hu et al, 2018. Comparison of Satellite-Derived Phytoplankton Size Classes Using In-
931 Situ Measurements in the South China Sea. Remote Sens. 10.
932 https://doi.org/10.3390/rs10040526.
933

934 Hu, C., Lee, Z., Franz, B., 2012. Chlorophyll a algorithms for oligotrophic oceans: A
935 novel approach based on three-band reflectance difference. J. Geophys. Res. Ocean. 117.
936 https://doi.org/10.1029/2011JC007395.
937
938 Ismael, A.A., 2015. Phytoplankton of the Red Sea. Springer, Berlin, Heidelberg, pp. 567–
939 583. https://doi.org/10.1007/978-3-662-45201-1_32.
940
941 Kheireddine, M., Ouhssain, M., Claustre, H., Uitz, J., Gentili, B., Jones, B.H., 2017.
942 Assessing Pigment-Based Phytoplankton Community Distributions in the Red Sea. Front.
943 Mar. Sci. 4, 132. https://doi.org/10.3389/fmars.2017.00132.
944
945 Kheireddine, M., Ouhssain, M., Organelli, E., Bricaud, A., & Jones, B. H. (2018a). Light
946 absorption by suspended particles in the Red Sea: effect of phytoplankton community
947 size structure and pigment composition. Journal of Geophysical Research: Oceans,
948 123(2), 902-921.
949
950 Kheireddine, M., Ouhssain, M., Calleja, M.L., Morán, X.A.G., Sarma, Y.V.B., Tiwari,
951 S.P., Jones, B.H., 2018b. Characterization of light absorption by chromophoric dissolved
952 organic matter (CDOM) in the upper layer of the Red Sea. Deep Sea Res. Part I
953 Oceanogr. Res. Pap. 133, 72–84. https://doi.org/10.1016/J.DSR.2018.02.001.
954

955 Kostadinov, T.S., Siegel, D.A., Maritorena, S., 2009. Retrieval of the particle size
956 distribution from satellite ocean color observations. J. Geophys. Res. Ocean. 114, 1–22.
957 https://doi.org/10.1029/2009JC005303.
958
959 Krokos, G., Papadopoulos, V.P., Sofianos, S.S., Ombao, H., Dybczak, P., Hoteit, I.,
960 2019. Natural Climate Oscillations may Counteract Red Sea Warming Over the Coming
961 Decades. Geophys. Res. Lett. 46, 3454–3461. https://doi.org/10.1029/2018GL081397
962
963 Lamont, T., Barlow, R.G., Brewin, R.J.W., 2018. Variations in remotely-sensed
964 phytoplankton size structure of a cyclonic eddy in the southwest Indian Ocean. Remote
965 Sens. 10. https://doi.org/10.3390/rs10071143.
966
967 Laws, E. A., Falkowski, P. G., Smith Jr, W. O., Ducklow, H., McCarth, J. J., 2000.
968 Temperature effects on export production in the open ocean, Global Biogeochem. Cycles
969 14, 1231–1246. doi:10.1029/1999GB001229.
970
971 Legendre, L., Le Fevre, J., 1991. From individual plankton cells to pelagic marine
972 ecosystems and to global biogeochemical cycles. In Particle analysis in oceanography.
973 Springer, Berlin, Heidelberg.
974

975 Lin, J., Cao, W., Wang, G., Hu, S., 2014. Satellite-observed variability of phytoplankton
976 size classes associated with a cold eddy in the South China Sea. Mar. Pollut. Bull. 83,
977 190–197. https://doi.org/10.1016/j.marpolbul.2014.03.052.
978
979 Liu, X., Devred, E., Johnson, C., 2018. Remote Sensing of Phytoplankton Size Class in
980 Northwest Atlantic from 1998 to 2016: Bio-Optical Algorithms Comparison and
981 Application. Remote Sens. 10(7), 1028. https://doi.org/10.3390/rs10071028.
982
983 Marañón, E., 2015. Cell Size as a Key Determinant of Phytoplankton Metabolism and
984 Community Structure. Ann. Rev. Mar. Sci. 7, 241–264. https://doi.org/10.1146/annurev-
985 marine-010814-015955.
986
987 Marañón, E., Cermeño, P., Latasa, M., Tadonléké, R.D., 2012. Temperature, resources,
988 and phytoplankton size structure in the ocean. Limnol. Oceanogr. 57, 1266–1278.
989 https://doi.org/10.4319/lo.2012.57.5.1266.
990
991 McCave, I., 1975. Vertical flux of particles in the ocean. Deep Sea Res. Oceanogr.
992 Abstr. 22(7), 491-502.
993
994 Moloney, C. L., Field, J. G., 1991. The size-based dynamics of plankton food webs. I. A
995 simulation model of carbon and nitrogen flows. J. Plankton Res. 13(5), 1003-1038.
996

997 Monroe, A. A., Ziegler, M., Roik, A., Röthig, T., Hardenstine, R.S., Emms, M.A.,
998 Jensen, T., Voolstra, C.R., Berumen, M.L., 2018. In situ observations of coral bleaching
999 in the central Saudi Arabian Red Sea during the 2015/2016 global coral bleaching
1000 event. PloS One 13(4), p.e0195814. https://doi.org/10.1371/journal.pone.0195814.
1001
1002 Morel, A., Gentili, B., 2009. The dissolved yellow substance and the shades of blue in the
1003 Mediterranean Sea. Biogeosciences 6, 2625–2636. https://doi.org/10.5194/bg-6-2625-
1004 2009.
1005
1006 Moses, W.J., Gitelson, A.A., Berdnikov, S., Saprygin, V., Povazhnyi, V., 2012.
1007 Operational MERIS-based NIR-red algorithms for estimating chlorophyll-a
1008 concentrations in coastal waters — The Azov Sea case study. Remote Sens. Environ.
1009 121, 118–124. https://doi.org/10.1016/j.rse.2012.01.024.
1010
1011 Mouw, C.B., Hardman-Mountford, N.J., Alvain, S., Bracher, A., Brewin, R.J.W.,
1012 Bricaud, A., Ciotti, A.M., Devred, E., Fujiwara, A., Hirata, T., Hirawake, T., Kostadinov,
1013 T.S., Roy, S., Uitz, J., 2017. A Consumer's Guide to Satellite Remote Sensing of
1014 Multiple Phytoplankton Groups in the Global Ocean. Front. Mar. Sci. 4.
1015 https://doi.org/10.3389/fmars.2017.00041.
1016
1017 Nair, A., Platt, T., Morales, J., Stuart, V., Forget, M.-H., Devred, E., Bouman, H., 2008.
1018 Remote sensing of phytoplankton functional types. Remote Sens. Environ. 112, 3366–
1019 3375. https://doi.org/10.1016/J.RSE.2008.01.021.

1020

1021 Nassar, M. Z., Mohamed, H. R., Khiray, H. M., Rashedy, S. H., 2014. Seasonal
1022 fluctuations of phytoplankton community and physico-chemical parameters of the north
1023 western part of the Red Sea, Egypt. Egypt J. Aquat. Res. 40(4), 395-403.
1024 https://doi.org/10.1016/j.ejar.2014.11.002.

1025

1026 Niemi, G. J., McDonald, M. E., 2004. Application of ecological indicators. Annu. Rev.
1027 Ecol. Evol. Syst. 35, 89-111.

1028

1029 O'Reilly, JE, Maritorena S, Siegel D, O'Brien MO, Toole D, Mitchell BG, Kahru M,
1030 Chavez F, Strutton PG, Cota GF, Hooker SB, McClain C, Carder K, Muller-Karger F,
1031 Harding L, Magnuson A, Phinney D, Moore G, Aiken J, Arrigo KR, Letelier RM, Culver
1032 M. 2000. Ocean color chlorophyll a algorithms for SeaWiFS, OC2, and OC4: Version 4.
1033 SeaWiFS Postlaunch Calibration and Validation Analyses. 11( McClain CR, Ed.).:9-23.,
1034 Greenbelt, Md.: Goddard Space Flight Center.

1035

1036 O'Reilly, J.E., Werdell, P.J., 2019. Chlorophyll algorithms for ocean color sensors - OC4,
1037 OC5 & OC6. Remote Sens. Environ. 229, 32–47.
1038 https://doi.org/10.1016/J.RSE.2019.04.021.

1039

1040 Organelli, E., Bricaud, A., Antoine, D., Matsuoka, A., 2014. Seasonal dynamics of light
1041 absorption by chromophoric dissolved organic matter (CDOM) in the NW Mediterranean

1042 Sea (BOUSSOLE site). Deep Sea Res. Part I Oceanogr. Res. Pap. 91, 72–85.
1043 https://doi.org/10.1016/J.DSR.2014.05.003.
1044
1045 Organelli, E., Bricaud, A., Antoine, D., Uitz, J., 2013. Multivariate approach for the
1046 retrieval of phytoplankton size structure from measured light absorption spectra in the
1047 Mediterranean Sea (BOUSSOLE site). Appl. Opt. 52, 2257.
1048 https://doi.org/10.1364/AO.52.002257.
1049
1050 Osman, E.O., Smith, D.J., Ziegler, M., Kürten, B., Conrad, C., El-Haddad, K.M.,
1051 Voolstra, C.R., Suggett, D.J., 2018. Thermal refugia against coral bleaching throughout
1052 the northern Red Sea. Glob. Change Biol. 24(2), 474-484.
1053 https://doi.org/10.1111/gcb.13895.
1054
1055 Papadopoulos, V.P., Zhan, P., Sofianos, S.S., Raitsos, D.E., Qurban, M., Abualnaja, Y.,
1056 Bower, A., Kontoyiannis, H., Pavlidou, A., Asharaf, T.T.M., Zarokanellos, N., Hoteit, I.,
1057 2015. Factors governing the deep ventilation of the Red Sea. J. Geophys. Res. Ocean.
1058 120, 7493–7505. https://doi.org/10.1002/2015JC010996.
1059
1060 Parsons, T. R., Lalli, C. M., 2002. Jellyfish population explosions: revisiting a hypothesis
1061 of possible causes. La mer. 40(3), 111-121.
1062

1063 Pearman, J.K., Kürten, S., Sarma, Y.V.B., Jones, B.H., Carvalho, S., 2016. Biodiversity
1064 patterns of plankton assemblages at the extremes of the Red Sea. FEMS Microbiol. Ecol.
1065 92, 1–13. https://doi.org/10.1093/femsec/fiw002.
1066
1067 Platt, T., Sathyendranath, S., 2008. Ecological indicators for the pelagic zone of the ocean
1068 from remote sensing. Remote Sens. Environ. 112(8), 3426–3436.
1069 http://doi.org/10.1016/j.rse.2007.10.016.
1070
1071 Platt, T., White III, G. N., Zhai, L., Sathyendranath, S., Roy, S., 2009. The phenology of
1072 phytoplankton blooms: Ecosystem indicators from remote sensing. Ecol. Model. 220(21),
1073 3057-3069. https://doi.org/10.1016/j.ecolmodel.2008.11.022.
1074
1075 Qurban, M.A.B., Wafar, M., Heinle, M., 2019. Phytoplankton and Primary Production in
1076 the Red Sea. Springer, Cham, pp. 491–506. https://doi.org/10.1007/978-3-319-99417-
1077 8_27.
1078
1079 Racault, M. F., Platt, T., Sathyendranath, S., Ağirbaş, E., Martinez Vicente, V., Brewin,
1080 R., 2014. Plankton indicators and ocean observing systems: Support to the marine
1081 ecosystem state assessment. J. Plankton Res. 36(3), 621–629.
1082 http://doi.org/10.1093/plankt/fbu016.
1083
1084 Racault, M.F., Platt, T., Sathyendranath, S., Ağirbaş, E., Martinez Vicente, V., Brewin,
1085 R., 2014. Plankton indicators and ocean observing systems: Support to the marine

ecosystem state assessment. J. Plankton Res. 36, 621–629. https://doi.org/10.1093/plankt/fbu016.

Racault, M.F., Raitsos, D.E., Berumen, M.L., Brewin, R.J.W., Platt, T., Sathyendranath, S., Hoteit, I., 2015. Phytoplankton phenology indices in coral reef ecosystems: Application to ocean-color observations in the Red Sea. Remote Sens. Environ. 160, 222–234. https://doi.org/10.1016/j.rse.2015.01.019.

Raimbault, P., 1988. Size fractionation of phytoplankton in the Ligurian Sea and the Algerian Basin (Mediterranean Sea): Size distribution versus total concentration. Mar. Microb. Food Webs 3, 1-7.

Raitsos, D.E., Brewin, R.J.W., Zhan, P., Dreano, D., Pradhan, Y., Nanninga, G.B., Hoteit, I., 2017. Sensing coral reef connectivity pathways from space. Sci. Rep. 7, 9338. https://doi.org/10.1038/s41598-017-08729-w.

Raitsos, D.E., Hoteit, I., Prihartato, P.K., Chronis, T., Triantafyllou, G., Abualnaja, Y., 2011. Abrupt warming of the Red Sea. Geophys. Res. Lett. 38, 1–5. https://doi.org/10.1029/2011GL047984.

1106 Raitsos, D.E., Pradhan, Y., Brewin, R.J.W., Stenchikov, G., Hoteit, I., 2013. Remote
1107 Sensing the Phytoplankton Seasonal Succession of the Red Sea. PLoS One 8.
1108 https://doi.org/10.1371/journal.pone.0064909.
1109
1110 Raitsos, D.E., Yi, X., Platt, T., Racault, M.F., Brewin, R.J.W., Pradhan, Y.,
1111 Papadopoulos, V.P.,Sathyendranath, S., Hoteit, I., 2015. Monsoon oscillations regulate
1112 fertility of the Red Sea. Geophys. Res. Lett. 42, 855–862.
1113 https://doi.org/10.1002/2014GL062882.
1114
1115 Ras, J., Claustre, H., Uitz, J., 2008. Spatial variability of phytoplankton pigment
1116 distributions in the Subtropical South Pacific Ocean: comparison between in situ and
1117 predicted data. Biogeosciences 5(2), 353-369. https://doi.org/10.5194/bg-5-353-2008.
1118
1119 Rasheed, M., Badran, M.I., Richter, C., Huettel, M., n.d. Effect of reef framework and
1120 bottom sediment on nutrient enrichment in a coral reef of the Gulf of Aqaba, Red Sea.
1121 Mar. Ecol. Prog. Ser. https://doi.org/10.2307/24866066.
1122
1123 Sammartino, M., Di Cicco, A., Marullo, S., Santoleri, R., 2015. Spatio-temporal
1124 variability of micro-, nano- and pico-phytoplankton in the Mediterranean Sea from
1125 satellite ocean colour data of SeaWiFS, Ocean Sci. 11, 759-778.
1126 https://doi.org/10.5194/os-11-759-2015.
1127

Sathyendranath, S. , Aiken, J. , Alvain, S. , Barlow, R. , Bouman, H. , Bracher, A. , Brewin, R. , Bricaud, A. , Brown, C. W. , Ciotti, A. M. , Clementson, L. A. , Craig, S. E. , Devred, E. , Hardman-Mountford, N. , Hirata, T. , Hu, C. , Kostadinov, T. S. , Lavender, S. , Loisel, H. , Moore, T. S. , Morales, J. , Mouw, C. B. , Nair, A. , Raitsos, D. , Roesler, C. , Shutler, J. D. , Sosik, H. M. , Soto, I. , Stuart, V. , Subramaniam, A. and Uitz, J. (2014): Phytoplankton functional types from Space. / S. Sathyendranath and V. Stuart (editors), (Reports of the International Ocean-Colour Coordinating Group (IOCCG); 15), Dartmouth, Nova Scotia, B2Y 4A2, Canada., International Ocean-Colour Coordinating Group, 156 p., ISBN: ISSN 1098-6030 .

Sathyendranath, S., Brewin, R.J.W., Brockmann, C., Brotas, V., Ciavatta, S., Chuprin, A., Couto, A.B., Doerffer, R., Dowell, M., Grant, M., 2016. Creating an ocean-colour time series for use in climate studies: The experience of the ocean-colour climate change initiative. Remote Sens. Env.

Sathyendranath, S., Brewin, B., Mueller, D., Doerffer, R., Krasemann, H., Melin, F., Brockmann, C., Fomferra, N., Peters, M., Grant, M., Steinmetz, F., Deschamps, P.-Y., Swinton, J., Smyth, T., Werdell, J., Franz, B., Maritorena, S., Devred, E., Lee, Z., Hu, C., Regner, P., 2012. Ocean Colour Climate Change Initiative — Approach and initial results, in: 2012 IEEE International Geoscience and Remote Sensing Symposium. IEEE, pp. 2024–2027. https://doi.org/10.1109/IGARSS.2012.6350979

1149

1150 Sathyendranath, S., Brewin, R.J.W., Jackson, T., Mélin, F., Platt, T., 2017. Ocean-colour
1151 products for climate-change studies: What are their ideal characteristics? Remote Sens.
1152 Environ. 203, 125–138. https://doi.org/10.1016/J.RSE.2017.04.017.
1153
1154 Sathyendranath, S., Cota, G., Stuart, V., Maass, H., Platt, T., 2001. Remote sensing of
1155 phytoplankton pigments: A comparison of empirical and theoretical approaches. Int. J.
1156 Remote Sens. 22, 249–273. https://doi.org/10.1080/014311601449925.
1157
1158 Sathyendranath, S., Platt, T., 2007. Spectral effects in bio-optical control on the ocean
1159 system, Oceanologia 49(1), 5–39.
1160
1161 Seegers, B.N., Stumpf, R.P., Schaeffer, B.A., Loftin, K.A., Werdell, P.J., 2018.
1162 Performance metrics for the assessment of satellite data products: an ocean color case
1163 study. Opt. Express 26, 7404. https://doi.org/10.1364/OE.26.007404.
1164
1165 Shaikh, E.A., Roff, J.C., Dowidar, N.M., 1986. Phytoplankton ecology and production in
1166 the Red Sea off Jiddah, Saudi Arabia. Mar. Biol. Int. J. Life Ocean. Coast. Waters 92,
1167 405–416. https://doi.org/10.1007/BF00392681.
1168
1169 Siegel, D.A., Behrenfeld, M.J., Maritorena, S., McClain, C.R., Antoine, D., Bailey, S.W.,
1170 Bontempi, P.S., Boss, E.S., Dierssen, H.M., Doney, S.C., Eplee, R.E., Evans, R.H.,
1171 Feldman, G.C., Fields, E., Franz, B.A., Kuring, N.A., Mengelt, C., Nelson, N.B., Patt,

F.S., Robinson, W.D., Sarmiento, J.L., Swan, C.M., Werdell, P.J., Westberry, T.K., Wilding, J.G., Yoder, J.A., 2013. Regional to global assessments of phytoplankton dynamics from the SeaWiFS mission. Remote Sens. Environ. 135, 77–91. https://doi.org/10.1016/J.RSE.2013.03.025.

Sommer, U., Berninger, U.G., Bottger-Schnack, R., Cornils, a, Hagen, W., Hansen, T., Al-Najjar, T., Post, a F., Schnack-Schiel, S.B., Stibor, H., Stubing, D., Wickham, S., 2002. Grazing during early spring in the Gulf of Aqaba and the Northern Red Sea. Mar. Ecol. Ser. 239, 251–261. https://doi.org/Doi 10.3354/Meps239251.

Sun, X., Shen, F., Liu, D., Bellerby, R. G., Liu, Y., Tang, R., (2018). In Situ and Satellite Observations of Phytoplankton Size Classes in the Entire Continental Shelf Sea, China. J. Geophys. Res. Ocean 123(5), 3523-3544. https://doi.org/10.1029/2017JC013651.

Touliabah, H. E., Abu El-Kheir, W. S., Kuchari, M. G., 2010. Phytoplankton composition at Jeddah Coast-Red Sea, Saudi Arabia in relation to some ecological factors. JKAU: Sci. 148(632), 1-34. doi:10.4197/Sci. 22-1.9.

Triantafyllou, G., Yao, F., Petihakis, G., Tsiaras, K.P., Raitsos, D.E., Hoteit, I., 2014. Exploring the Red Sea seasonal ecosystem functioning using a three-dimensional biophysical model. J. Geophys. Res. Ocean. 119, 1791–1811. https://doi.org/10.1002/2013JC009641.

1195 Uitz, J., Claustre, H., Morel, A., Hooker, S.B., 2006. Vertical distribution of
1196 phytoplankton communities in open ocean: An assessment based on surface chlorophyll.
1197 J. Geophys. Res. Ocean. 111. https://doi.org/10.1029/2005JC003207.
1198
1199 Uitz, J., Stramski, D., Reynolds, R.A., Dubranna, J., 2015. Assessing phytoplankton
1200 community composition from hyperspectral measurements of phytoplankton absorption
1201 coefficient and remote-sensing reflectance in open-ocean environments. Remote Sens.
1202 Environ. 171. https://doi.org/10.1016/j.rse.2015.09.027.
1203
1204 Uitz, J.U., Huot, Y., Bruyant, F., Babin, M., Claustre, H., 2008. Relating phytoplankton
1205 photophysiological properties to community structure on large scales. Limnol. Oceanogr.
1206 53, 614–630. https://doi.org/10.4319/lo.2008.53.2.0614.
1207
1208 Vidussi, F., Claustre, H., Manca, B.B., Luchetta, A., Jean-Claude, M., 2001.
1209 Phytoplankton pigment distribution in relation to upper thermocline circulation in the
1210 eastern Mediterranean Sea during winter. J. Geophys. Res. 106, 939–956.
1211 https://doi.org/10.1029/1999JC000308.
1212
1213 Ward, B. A., 2015. Temperature-correlated changes in phytoplankton community
1214 structure are restricted to polar waters. PloS one 10(8), e0135581.
1215

Willmott, C., Matsuura, K., 2005. Advantages of the mean absolute error (MAE) over the root mean square error (RMSE) in assessing average model performance. Clim. Res. 30, 79–82. https://doi.org/10.3354/cr030079.

Zhan, P., Subramanian, A.C., Yao, F., Hoteit, I., 2014. Eddies in the Red Sea: A statistical and dynamical study. J. Geophys. Res. Ocean. 119, 3909–3925. https://doi.org/10.1002/2013JC009563.

Zhan, P., Krokos, G., Guo, D., Hoteit, I., 2019. Three-Dimensional Signature of the Red Sea. Eddies and Eddy-Induced Transport. Geophys. Res. Lett. 46, 2167–2177. https://doi.org/10.1029/2018GL081387.

## ACKNOWLEDGMENTS

The authors are grateful to the Ocean Colour CCI team (European Space Agency) for providing and processing the Chl-a dataset. The authors also thank Nick Selmes for processing and providing the Sentinel-3 OLCI Chl-a dataset for the Red Sea. The authors express their gratitude to the scientists, officers and crews of the *R/V Thuwal*, the KAUST Coastal and Marine Resources Core Lab who provided logistical support and assistance during fieldwork, and the Analytical Core Lab for providing facilities for the analyses of

the samples collected during the fieldwork. The authors are grateful to Benjamin Kurten, Susana Carvalho, Sarma Yellepeddi, and Joanne Ellis for facilitating the sampling of optical and pigment samples for the research cruises listed. The authors also thank George Krokos for his useful discussions. This work was funded by the KAUST Office of Sponsored Research (OSR) under the Collaborative Research Grant (CRG) program (Grant # URF/1/2979-01-01) and the Virtual Red Sea Initiative (Grant # REP/1/3268-01-01). Fieldwork was supported by KAUST baseline funding (BAS/1/1032-01-01) attributed to Burton Jones.

## AUTHOR CONTRIBUTIONS

J.A.G., R.J.W.B., D.R.E. & I.H. designed the research. J.A.G., R.J.W.B. & D.R.E. carried out the data analysis. J.A.G. wrote the paper. J.A.G., R.J.W.B., & D.R.E. produced the figures. J.A.G., R.J.W.B., D.R.E., M.K., M.O., B.H.J. & I.H. contributed to the interpretation of results, the discussion and subsequent edits of the paper.